Available online at www.sciencedirect.com
SCIENCE DIRECT
Coordination Chemistry Reviews 250 (2006) 1681–1695
COORDINATION CHEMISTRY REVIEWS
www.elsevier.com/locate/ccr

Review

Kinetic studies of the photoinduced formation of transition metal–dinitrogen complexes using time-resolved infrared and UV–vis spectroscopy

David C. Grills, Kuo-Wei Huang, James T. Muckerman, Etsuko Fujita *

Chemistry Department, Brookhaven National Laboratory, Upton, NY 11973-5000, USA

Received 15 September 2005; accepted 3 January 2006
Available online 9 February 2006

Contents

Abstract

Previous kinetic studies of photoinitiated transition metal–dinitrogen bond forming reactions are reviewed, with an emphasis on room temperature reactivity, and in particular, the techniques of time-resolved infrared (TRIR) spectroscopy and UV–vis flash photolysis. Our recent results on the reactivity of the formally 16-electron, but agostically stabilized, complex, *mer*,*trans*-$W(CO)_3(PCy_3)_2$ (**W**) (Cy = cyclohexyl) toward N_2 in toluene and *n*-hexane solution are then discussed. Laser flash photolysis of a toluene solution of **W**-N_2 in the presence of excess N_2 resulted in the photoejection of N_2. The back reaction of **W** with N_2 was followed by monitoring the decay of the transient absorption of **W** at 600 nm. The second-order rate constant for the reaction of N_2 with **W** in toluene to generate **W**–N_2 was found to be $(3.0 \pm 0.2) \times 10^5\ M^{-1}\ s^{-1}$. The rate of the reverse reaction was found to be $100 \pm 10\ s^{-1}$, allowing an estimation of the equilibrium constant, $K_{N_2} = (3.0 \pm 0.5) \times 10^3\ M^{-1}$. Time-resolved step-scan FTIR (s^2-FTIR) spectroscopy was also used to spectroscopically characterize the **W** intermediate and monitor its back-reaction with N_2 in *n*-hexane solution. The rate of formation of **W**–N_2 measured by s^2-FTIR agreed well with that measured by flash photolysis. Finally, density functional theory (DFT) calculations have been performed on the model complexes, *mer*,*trans*-$W(CO)_3(PH_3)_2(L)$ (L = none and N_2) in order to understand the observed IR and UV–vis spectra of **W** and **W**–N_2 and to determine the nature of the frontier molecular orbitals of **W** and **W**–N_2, allowing their lowest energy excited states to be assigned.

Keywords: Nitrogen fixation; Dinitrogen complex; Time-resolved Infrared; Flash photolysis; Binding rates

1. Introduction

Since the first observation of a transition metal dinitrogen complex, $[Ru(N_2)(NH_3)_5]^{2+}$, in 1965 [1], a wide variety of

* Corresponding author. Tel.: +1 631 344 4356; fax: +1 631 344 5815.
E-mail address: fujita@bnl.gov (E. Fujita).

0010-8545/$ – see front matter © 2006 Elsevier B.V. All rights reserved.
doi:10.1016/j.ccr.2006.01.002

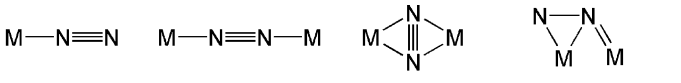

Scheme 1.

metal–dinitrogen compounds have been synthesized and characterized. This is due to intense interest in and the importance of the development of chemical nitrogen fixation systems [2–5]. Some of the binding modes that are observed for dinitrogen to transition metals are shown in Scheme 1 [5]. By far the most commonly observed of these is end-on mononuclear.

Nitrogen fixation is the process in which the relatively inert molecular gas, dinitrogen is converted into nitrogen-containing compounds that are extremely useful for other chemical processes, e.g. ammonia, nitrates and nitrogen dioxide. Nature has perfected this process over millions of years, with biological nitrogen fixation taking place in the iron–molybdenum nitrogenase bacterial enzymes [6], many of which enjoy a symbiotic relationship with legume plants. Chemical nitrogen fixation, in which nitrogen gas is artificially fixed into useful chemicals, particularly fertilizers, is an extremely important industrial process. The most common form of chemical nitrogen fixation used today is the Haber–Bosch process [7], in which nitrogen and hydrogen gas are reacted over an iron-based catalyst at 400–650 °C and 200–400 atm to produce gaseous ammonia, which is then used as a chemical feedstock. However, the precise mechanism of this catalytic reaction is still not fully understood and the reaction conditions are rather harsh. The ultimate goal would be to develop a transition metal-based chemical nitrogen fixation catalyst that could efficiently convert gaseous nitrogen into ammonia or other useful nitrogen compounds at, or close to, ambient conditions, possibly using solar produced electrons and protons rather than molecular hydrogen.

In order to develop such a catalyst, all of the reaction steps that could potentially be involved in the catalytic cycle must be fully understood. One important primary step would involve the non-dissociative binding of dinitrogen to a coordinatively unsaturated metal center in the catalyst, to generate a transition metal–dinitrogen complex. A deeper understanding of the interaction between coordinated dinitrogen and metal centers, including the rates and thermodynamics of formation, structures, bonding properties and reactivities toward other reagents, is therefore required in order to advance the development of nitrogen fixation catalysts. Multiple factors, such as solvation of the metal center, the particular ligand environment (i.e., agostic, steric and electronic effects) and the nature of the metal center, including its oxidation state and spin multiplicity, can have a major influence on the rate and selectivity of a transition metal–dinitrogen binding process and hence on the potential of such a species to act as an efficient catalyst. All of these factors need to be examined in detail in order to aid the development of the next generation of chemical nitrogen fixation catalysts.

A convenient route to coordinatively unsaturated transition metal fragments is via the photolytic cleavage of a ligand from some precursor complex using a source of UV–vis light e.g. a xenon lamp or a laser. If dinitrogen is present in the reaction vessel, it may then react with the unsaturated metal fragment to form a transition metal–dinitrogen complex. One set of compounds that have been successfully employed in such studies are the transition metal carbonyls [8,9]. UV excitation of a transition metal carbonyl compound often produces a ligand field excited state, which results in the cleavage of a CO molecule and the generation of a highly reactive, coordinatively unsaturated metal fragment, which can then react with dinitrogen (see equations below, where L represents one or more peripheral ligands),

$$\mathrm{LM(CO)}_x \overset{h\nu}{\rightleftharpoons} \mathrm{LM(CO)}_{x-1} + \mathrm{CO}$$

$$\mathrm{LM(CO)}_{x-1} + \mathrm{N_2} \overset{k_{\mathrm{N_2}}}{\rightleftharpoons} \mathrm{LM(CO)}_{x-1}(\mathrm{N_2})$$

It should be noted that in solution, the unsaturated metal center will generally be solvated, with a molecule of the solvent behaving as a weak "token" ligand at the vacant coordination site [10]. This solvation occurs on the pico- or sub-picosecond timescale [11] and therefore dinitrogen will actually be reacting with the solvated species rather than the nascent unsaturated fragment. However, exceptions to this rule do occur and some of these will be discussed later. Transition metal dihydride complexes with mutually *cis* hydride ligands are also a useful alternative to metal carbonyls [12]. Photolysis of these hydrides results in the elimination of molecular hydrogen and the formation of an unsaturated metal fragment. The highly reactive nature of coordinatively unsaturated transition metal fragments presents certain challenges with regards to their characterization and identification and for monitoring the rates of their reactions with incoming ligands, such as dinitrogen. Such bimolecular reactions will often occur on timescales as fast as nanoseconds at room temperature. The traditional method of overcoming these difficulties has been to use cryogenic media, such as frozen inert gas matrices or liquefied noble gases, which stabilize the reactive photofragments and photoproducts to such a degree that they can be monitored at leisure by conventional spectroscopic techniques like IR, UV–vis and EPR spectroscopy. Indeed, much of our current knowledge about unsaturated transition metal fragments is based upon the elegant results of early matrix isolation experiments. However, only very limited, if any, kinetic information can be obtained from such cryogenic studies. If better catalytic systems are to be developed, it is desirable to obtain experimental information regarding the reactivity of unsaturated metal fragments toward dinitrogen at or above room temperature. In the last 20–30 years, time-resolved spectroscopic techniques have improved dramatically, thus allowing the reactions of dinitrogen with transition metal centers to be followed in real time at room temperature, revealing the dinitrogen binding rates and other thermodynamic information about the bond forming process. In the following section, these techniques will be discussed briefly.

1.1. Introduction to TRIR and flash photolysis

As mentioned above, directly monitoring the reaction of dinitrogen with a coordinatively unsaturated transition metal

fragment requires the use of a fast technique that can operate on timescales ranging from nano- to microseconds. In 1949, Norrish and Porter developed the technique of flash photolysis for the spectroscopic study of photogenerated reactive species on the microsecond timescale [13]. In their experiments, a gas-discharge flashlamp was used to initiate a photochemical reaction and a second, smaller flashlamp, was used to probe changes in the UV–vis spectrum following the flash, with photographic film as the detector. With the advent of modern pulsed lasers and fast UV–vis detectors, the technique of flash photolysis has become invaluable for monitoring the dynamics of photochemical reactions on timescales as short as femtoseconds [14]. However, a severe limitation of conventional flash photolysis when applied to species such as transition metal carbonyls is the broad, featureless nature of the UV–vis absorption bands that are observed. Thus, little or no structural information can be obtained about the reactive intermediates under study. However, the complementary technique of time-resolved infrared (TRIR) spectroscopy, a combination of flash photolysis and fast infrared detection, does provide excellent structural information [15]. IR absorption bands, particularly those of metal carbonyls, are intense and narrow, and their frequencies and intensities are extremely sensitive to the structure of the metal complex. In some cases, analysis of the IR absorption bands can even provide an accurate estimate of bond angles within the metal complex [16].

The initial development of TRIR spectroscopy was hampered, relative to flash photolysis, by poor IR light sources and inferior detector technology. However, improvements in these areas have since led to a series of powerful, modern TRIR techniques that permit the IR absorption spectra of reactive intermediates to be measured on timescales ranging from femto- to milliseconds [17]. In this paper we shall focus on nano- to millisecond TRIR (so-called, 'fast' TRIR) since this is the timescale on which bimolecular reactions of dinitrogen with transition metal fragments occur in the gas and condensed phases at room temperature. There are two general techniques for fast TRIR spectroscopy; dispersive, or 'point-by-point' TRIR [15,17,18] and step-scan FTIR [19–23]. Dispersive TRIR was the original method of TRIR spectroscopy and is still the most commonly used today. It typically employs either a conventional globar (a black body source) or a continuous wave IR laser as the source of IR probe light. When a globar is used, it is equipped with a monochromator that selects an individual IR frequency with which to probe the reaction mixture as a function of time following laser flash photolysis. More commonly nowadays, an IR diode laser/monochromator or a CO laser is used as the IR light source. These IR laser-based systems offer several advantages over globar based systems [18]. However, modern TRIR spectrometers with globar sources are still used, with excellent results being obtained [24–27]. In dispersive TRIR, individual kinetic traces monitoring the change in absorbance of the sample at particular IR frequencies are built up on a point-by-point basis. The kinetic traces are then combined and time slices taken to reveal TRIR difference spectra at any desired time interval after photolysis. However, this technique, although it provides extremely detailed kinetic information at precise IR frequencies, is rather labor intensive. Step-scan FTIR spectroscopy has improved dramatically in recent years and has become a viable alternative to dispersive TRIR. In step-scan FTIR, the moving mirror of a conventional FTIR interferometer is moved stepwise in discrete steps. At each mirror position, the mirror is held stationary, the sample is excited by a laser flash and the change in intensity of the interferogram at that mirror position is monitored as a function of time. If required, signal averaging can be performed by repeating the measurement with multiple laser shots and then the computer moves the mirror to its next position and so on, until a complete time-resolved interferogram has been constructed, from which high quality time-resolved FTIR difference spectra can be generated. Advantages of step-scan FTIR are that it is a fully automated, computer controlled technique and high quality FTIR spectra, covering the entire mid-IR region can be obtained in a single experiment on timescales down to 10 ns. A disadvantage of step-scan FTIR is the large number of laser shots that are required to complete a single experiment. Thus, the sample must be either extremely photoreversible or it must be recycled using a flow system during the experiment. Therefore, dispersive TRIR and step-scan FTIR complement one another and parallel access to both of these techniques in the same laboratory is highly desirable.

1.2. Previously measured dinitrogen binding rates using TRIR and flash photolysis

1.2.1. Gas-phase studies

Dinitrogen binding to transition metal centers has been well studied in the gas phase by both UV–vis flash photolysis and TRIR spectroscopy. An advantage of performing these experiments in the gas phase is that it is a solvent-free environment, thus eliminating the effect of solvent coordination at the metal center, allowing the coordination of dinitrogen to truly "naked", unsaturated metal fragments to be easily monitored by changes in both the observed spectra and kinetics upon addition of dinitrogen gas. Due to the lower frequency of collisional deactivation processes in the gas phase compared to in solution, the photogenerated intermediates are often formed in vibrationally excited states, which can sometimes complicate their IR spectra and also induce multiple ligand dissociations and hence reaction products. However, a number of gas-phase studies have been performed, which have contributed greatly to our understanding of the kinetics and thermodynamics of the transition metal–dinitrogen binding process. We do not intend to exhaustively review all of the gas-phase studies in the literature, but rather wish to highlight some of the prominent examples, focusing in particular on the application of TRIR spectroscopy to obtain kinetic data.

Gas-phase TRIR kinetic studies on the binding rate constants of dinitrogen to $W(CO)_5$, $W(CO)_4$, and $W(CO)_4(N_2)$ were carried out by monitoring the disappearance of these photogenerated tungsten carbonyl intermediates and the formation of the resulting dinitrogen complexes, $W(CO)_5(N_2)$, $W(CO)_4(N_2)$, and $W(CO)_4(N_2)_2$, respectively, following laser flash photolysis of $W(CO)_6$ in the presence of N_2 [28]. XeCl excimer laser photolysis (308 nm) of $W(CO)_6$ in the gas phase generates $W(CO)_5$,

which exhibits two ν(CO) IR bands at 1980 and 1942 cm^{-1} [29]. The growth of a new band at 1985 cm^{-1} was observed, concurrent with the decay of $W(CO)_5$ on the ns–μs timescale. The new band was assigned to the ν(CO) mode of $W(CO)_5(N_2)$ having *E* symmetry (see Table 1), by comparison with the solution phase IR spectrum of its Cr analogue, $Cr(CO)_5(N_2)$ [30]. The bimolecular rate constant for dinitrogen binding to $W(CO)_5$ ($k_{N_2} = (3.4 \pm 0.9) \times 10^{-11}$ cm^3 $molecule^{-1}$ s^{-1}) was derived from the observed rates of decay of $W(CO)_5$ (at 1972 cm^{-1}) and growth of $W(CO)_5(N_2)$ (at 1985 cm^{-1}) as a function of nitrogen pressure (0.1–1.5 Torr), while keeping that of $W(CO)_6$ (10 mTorr) and the overall pressure (10 Torr buffered by Ar) constant (see Table 1). In addition, H_2 and D_2 binding rates to $W(CO)_5$ were measured in this manner. Interestingly, the relative reactivity of gas-phase $W(CO)_5$ with N_2, H_2, and D_2 was found to be similar to that of the $Cr(CO)_5$(cyclohexane) solvated complex in cyclohexane solution (see later). $W(CO)_5(N_2)$ was found to have a lifetime greater than 1 ms (the observation limit of their apparatus), which, by following a simplified statistical mechanical analysis, suggested that the W–N_2 binding energy is greater than 16 kcal mol^{-1} under the gas-phase reaction conditions.

KrF excimer laser photolysis (248 nm) of gas-phase $W(CO)_6$ produces $W(CO)_4$ as the main photoproduct [29]. Following vibrational cooling of the initially generated "hot" $W(CO)_4$, this molecule exhibited ν(CO) IR bands at 1949 and 1919 cm^{-1} [28]. When N_2 was added, two new bands at 1925 and 1963 cm^{-1}, assigned to $W(CO)_4(N_2)$, were observed to grow in as the bands of $W(CO)_4$ disappeared. Subsequently, these two bands decayed concurrent with the growth of another new band at 1973 cm^{-1}, which was assigned to the formation of $W(CO)_4(N_2)_2$. Once again, the life time of the final species, $W(CO)_4(N_2)_2$, was found to be greater than 1 ms. Nitrogen pressure dependence experiments were performed in order to obtain the bimolecular rate constants for N_2 binding. All of the kinetic data and IR frequencies are summarized in Table 1, together with the reaction probabilities estimated by the authors, assuming collision diameters of 0.75 nm for $W(CO)_5$ and $W(CO)_4(N_2)$, 0.70 nm for $W(CO)_4$, and 0.38 nm for N_2 [31]. The large reaction probabilities indicate that the coordination of N_2 to the coordinatively unsaturated $W(CO)_x$ ($x = 4$ or 5) species has little or no barrier in the gas phase. The faster binding rate of N_2 to $W(CO)_4$ than to $W(CO)_5$ could be a result of a less crowded and more electron-rich tungsten center.

In similar experiments using $Fe(CO)_5$, the binding rate constants of molecular dinitrogen to the unsaturated intermediates, $Fe(CO)_3$, $Fe(CO)_4$, and $Fe(CO)_3(N_2)$ were measured using TRIR [32,33]. For the addition of N_2 to $Fe(CO)_3$ [32], the experiments were conducted under 50 mTorr of $Fe(CO)_5$, 0–100 mTorr of N_2, and buffer He to bring the total pressure to 90 Torr. $Fe(CO)_3$ was generated upon 308 nm XeCl excimer laser photolysis of the $Fe(CO)_5$. The rate constant was determined by following the N_2 pressure dependent decay of $Fe(CO)_3$ monitored by its 1950 cm^{-1} ν(CO) band (see Table 1). Although the formation of $Fe(CO)_3(N_2)$ could potentially be monitored at 1966 cm^{-1}, no accurate analysis could be performed due to the extensive convolution of this signal by another that was generated by a further reaction of $Fe(CO)_3(N_2)$ on a similar timescale. However, the rate of decrease of $Fe(CO)_3$ and the rate of growth of $Fe(CO)_3(N_2)$ proceeded on a common timescale when compared visually. The rate constant, $(2.5 \pm 1.0) \times 10^{-11}$ cm^3 $molecule^{-1}$ s^{-1} [32], is comparable to those obtained for the addition of N_2 to the unsaturated tungsten carbonyls discussed above [28] (see Table 1).

For the reaction of N_2 with $Fe(CO)_4$, the experiments were conducted under 50 mTorr of $Fe(CO)_5$, 0.0–18.4 Torr of N_2, ~9 Torr of CO, and He to bring the total pressure to 90 Torr. $Fe(CO)_4$ was produced by the addition of CO to the $Fe(CO)_3$ that was photolytically generated by the 308 nm laser photolysis of $Fe(CO)_5$ [32]. The rate constant for the addition of N_2 to $Fe(CO)_4$ was determined by following the N_2 pressure dependent decay of $Fe(CO)_4$ monitored by its 1981 cm^{-1} ν(CO) band.

Table 1
Second-order rate constants, k_{N_2} for the gas-phase reactions of N_2 with various photolytically generated coordinatively unsaturated metal carbonyl fragments, measured by TRIR spectroscopy

Reaction (estimated reaction probability)	Product	Rate constant (cm^3 $molecule^{-1}$ s^{-1})	Rate constant (M^{-1} s^{-1})[a]	Observed ν(CO) IR frequencies of the product (cm^{-1})[b]	Ref.
$W(CO)_5 + N_2$ (0.06 ± 0.02)	$W(CO)_5(N_2)$	$(3.4 \pm 0.9) \times 10^{-11}$[c]	$(2.0 \pm 0.6) \times 10^{10}$	1985 (E), 1974sh (A_1)	[28]
$W(CO)_4 + N_2$ (0.14 ± 0.03)	$W(CO)_4(N_2)$	$(6.8 \pm 1.5) \times 10^{-11}$[c]	$(4.1 \pm 0.9) \times 10^{10}$	1963 (B_1, A_1), 1925 (B_2)	[28]
$W(CO)_4(N_2) + N_2$ (0.03 ± 0.01)	$W(CO)_4(N_2)_2$	$(1.9 \pm 0.3) \times 10^{-11}$[c]	$(1.1 \pm 0.2) \times 10^{10}$	1973	[28]
$Fe(CO)_3 + N_2$	$Fe(CO)_3(N_2)$	$(2.5 \pm 1.0) \times 10^{-11}$	$(1.5 \pm 0.6) \times 10^{10}$	1973, 1966	[32]
$Fe(CO)_4 + N_2$	$Fe(CO)_4(N_2)$	$(2.8 \pm 0.2) \times 10^{-14}$	$(1.7 \pm 0.1) \times 10^{7}$	1992, 1984	[32]
$Fe(CO)_3(N_2) + N_2$	$Fe(CO)_3(N_2)_2$	$(5.4 \pm 1.8) \times 10^{-16}$	$(3.3 \pm 1.1) \times 10^{5}$	2026, 1992, 1985sh	[33]
(η^6-C_6H_6)$Cr(CO)_2 + N_2$	(η^6-C_6H_6)$Cr(CO)_2(N_2)$	$(4.3 \pm 0.3) \times 10^{-12}$[d]	$(2.6 \pm 0.2) \times 10^{9}$	1963 (A′), 1922 (A″)	[38]
(η^6-C_6H_6)$Cr(CO) + N_2$	(η^6-C_6H_6)$Cr(CO)(N_2)$	$(2.2 \pm 0.2) \times 10^{-13}$[d]	$(1.3 \pm 0.1) \times 10^{8}$	ν(CO) not observed	[38]
$CpMn(CO)_2 + N_2$	$CpMn(CO)_2(N_2)$	$(6.1 \pm 0.7) \times 10^{-13}$[d]	$(3.7 \pm 0.4) \times 10^{8}$	1997 (A′), 1948 (A″)	[38]
$CpMn(CO) + N_2$	$CpMn(CO)(N_2)$	$\leq 1.7 \times 10^{-12}$[d]	$\leq 1.0 \times 10^{9}$	ν(CO) not observed	[38]

[a] We have converted all of the rate constants into units of M^{-1} s^{-1} in order to allow for a comparison with the solution phase rate constants that are discussed later.
[b] Symmetries of some of the bands are shown in parentheses.
[c] Originally reported in $Torr^{-1}$ s^{-1} but we have converted to cm^3 $molecule^{-1}$ s^{-1}, based on an assumption that the kinetic studies were conducted at 298.15 K.
[d] Originally reported in cm^3 mol^{-1} s^{-1}. sh: shoulder.

The rate constant, $(2.8 \pm 0.2) \times 10^{-14}$ cm^3 molecule^{-1} s^{-1}, is significantly slower than that observed for the addition of N_2 to $Fe(CO)_3$ and other unsaturated transition metal carbonyl fragments [32] (see Table 1). For comparison, the addition of H_2, CO, and C_2H_4 to $Fe(CO)_4$ all occur at similar rates, with rate constants of $(5.9 \pm 1.5) \times 10^{-14}$, $(5.8 \pm 1.5) \times 10^{-14}$, and $(1.7 \pm 0.2) \times 10^{-13}$ cm^3 molecule^{-1} s^{-1}, respectively [34–36]. These slow rates can most likely be attributed to the change in spin multiplicity that occurs on addition of a ligand, L to $Fe(CO)_4$ to go from the triplet ground state of $Fe(CO)_4$ to the singlet ground state of $Fe(CO)_4L$ [37].

As discussed above, $Fe(CO)_3(N_2)$ could potentially be monitored at 1966 cm^{-1}, but under the experimental conditions, the signal was convoluted with a further reaction of $Fe(CO)_3(N_2)$ and no accurate kinetic data could be obtained [32]. However, in a later study in the same laboratory [33], the complicated results were successfully analyzed by fitting data for the dependence of the rate of disappearance of $Fe(CO)_3(N_2)$ on the pressures of N_2 and $Fe(CO)_5$. It appeared to contain two competitive reaction pathways that consume the transient $Fe(CO)_3(N_2)$ species,

$$Fe(CO)_3(N_2) + N_2 \rightarrow Fe(CO)_3(N_2)_2$$

$$Fe(CO)_3(N_2) + Fe(CO)_5 \rightarrow Fe_2(CO)_8(N_2)$$

The rate constants obtained were $(5.4 \pm 1.8) \times 10^{-16}$ cm^3 molecule^{-1} s^{-1} and $(4.3 \pm 2.2) \times 10^{-13}$ cm^3 molecule^{-1} s^{-1} for N_2 addition to $Fe(CO)_3(N_2)$ and $Fe(CO)_5$ addition to $Fe(CO)_3(N_2)$, respectively (see Table 1). The reaction of N_2 with $Fe(CO)_3(N_2)$ appeared to be unique with respect to other addition reactions of small ligands to coordinatively unsaturated metal carbonyls, which are typically unactivated, in that their data were consistent with this process having an activation energy of 5.7 ± 3.6 kcal mol^{-1}, thus leading to the extremely small rate constant.

The gas-phase binding rates of dinitrogen to coordinatively unsaturated transition metal fragments that contain other ligands, in addition to CO, have also been measured. For example, Fu and coworkers used TRIR spectroscopy to obtain kinetic data for the coordination of dinitrogen to $(\eta^6\text{-}C_6H_6)Cr(CO)_x$ and $CpMn(CO)_x$ ($x = 1$ and 2; $Cp = \eta^5\text{-}C_5H_5$) [38]. $(\eta^6\text{-}C_6H_6)Cr(CO)_2$ was generated by flash photolysis of $(\eta^6\text{-}C_6H_6)Cr(CO)_3$ using a frequency tripled (355 nm) Nd:YAG laser. Monitoring the pseudo-first-order decay of $(\eta^6\text{-}C_6H_6)Cr(CO)_2$ at 1981 cm^{-1} and growth of $(\eta^6\text{-}C_6H_6)Cr(CO)_2(N_2)$ at 1963 cm^{-1} following laser flash photolysis of mixtures of 10 mTorr of $(\eta^6\text{-}C_6H_6)Cr(CO)_3$, 0.5–3.0 Torr of N_2, and 10 Torr of Ar, gave a second-order rate constant for the formation of $(\eta^6\text{-}C_6H_6)Cr(CO)_2(N_2)$, $k_{N_2} = (4.3 \pm 0.3) \times 10^{-12}$ cm^3 molecule^{-1} s^{-1}. This rate constant is comparable to those for the reactions of N_2 with other coordinatively unsaturated transition metal carbonyl complexes in the gas phase (see Table 1). $(\eta^6\text{-}C_6H_6)Cr(CO)$ was produced as the major photoproduct (5:2 mixture with $(\eta^6\text{-}C_6H_6)Cr(CO)_2$) following 266 nm laser irradiation of $(\eta^6\text{-}C_6H_6)Cr(CO)_3$. An absorption band at ~1984 cm^{-1}, observed in the TRIR spectra, was assigned to the ν(CO) of $(\eta^6\text{-}C_6H_6)Cr(CO)$ overlapped with the A_1 band of $(\eta^6\text{-}C_6H_6)Cr(CO)_2$. In the presence of N_2, the 1984 cm^{-1} band was observed to decay via double exponential kinetics. No new absorption band was located that could be positively assigned to the formation of $(\eta^6\text{-}C_6H_6)Cr(CO)(N_2)$. However, this was believed to be due to obstruction from the much stronger bands of $(\eta^6\text{-}C_6H_6)Cr(CO)_2(N_2)$ and $(\eta^6\text{-}C_6H_6)Cr(CO)_3$. The fast component of the 1984 cm^{-1} decay was readily assigned to the reaction of $(\eta^6\text{-}C_6H_6)Cr(CO)_2$ with N_2, while the slow component was assigned to the reaction of $(\eta^6\text{-}C_6H_6)Cr(CO)$ with N_2. A plot of the N_2-pressure dependence of the slower component of the 1984 cm^{-1} decay gave a rate constant for the binding of dinitrogen to $(\eta^6\text{-}C_6H_6)Cr(CO)$ to generate $(\eta^6\text{-}C_6H_6)Cr(CO)(N_2)$, $k_{N_2} = (2.2 \pm 0.2) \times 10^{-13}$ cm^3 molecule^{-1} s^{-1} (see Table 1). The much slower rate compared to that of $(\eta^6\text{-}C_6H_6)Cr(CO)_2$ is likely the result of a spin-disallowed process, similar to the above-mentioned dinitrogen coordination reactions to iron carbonyl complexes. Laser flash photolysis (355 nm) of $CpMn(CO)_3$ afforded both of the coordinatively unsaturated fragments, $CpMn(CO)_2$ and $CpMn(CO)$. $CpMn(CO)_2$ exhibited two ν(CO) absorption bands at 1874 and 2021 cm^{-1}, and $CpMn(CO)$ featured a band at 1948 cm^{-1}. The N_2-pressure dependence of the decay of $CpMn(CO)_2$ and the growth of $CpMn(CO)_2(N_2)$ was monitored at 1874 and 1997 cm^{-1}, respectively, without added Ar buffer gas because of the potential coordination of Ar to $CpMn(CO)_2$. A second-order rate constant for dinitrogen binding to $CpMn(CO)_2$, $k_{N_2} = (6.1 \pm 0.7) \times 10^{-13}$ cm^3 molecule^{-1} s^{-1} was obtained (see Table 1), which was also comparable to the rate of a spin-disallowed process. Laser flash photolysis (266 nm) of $CpMn(CO)_3$ was found to generate $CpMn(CO)$ as the only observable photoproduct. However, no N_2-pressure dependence for the decay of this species could be observed. This was presumed to be due to a fortuitous spectral overlap of the ν(CO) bands of $CpMn(CO)$ and $CpMn(CO)(N_2)$. Due to the complexity of the TRIR spectra, only an upper limit could be estimated for the binding rate of N_2 to $CpMn(CO)$, $k_{N_2} \leq 1.7 \times 10^{-12}$ cm^3 molecule^{-1} s^{-1} (see Table 1). However, this is greater than that for addition to $CpMn(CO)_2$ and it was therefore assumed that the coordination of dinitrogen to $CpMn(CO)$ is a spin-allowed process. Both $(\eta^6\text{-}C_6H_6)Cr(CO)_2(N_2)$ and $CpMn(CO)_2(N_2)$ were found to have lifetimes greater than 1 ms, which on the basis of a simplified statistical mechanical analysis, suggested that the Cr–N_2 and Mn–N_2 binding energies were greater than 17 kcal mol^{-1}.

1.2.2. Condensed-phase studies

The binding of dinitrogen to transition metal centers in the condensed phase has been extensively investigated. In the majority of this work cryogenic media, such as frozen dinitrogen matrices [39] or liquefied noble gases doped with N_2 [40,41], have been used in order to stabilize the dinitrogen complexes and their unsaturated precursors sufficiently to allow their study by conventional spectroscopic techniques. Even supercritical fluids, such as supercritical Xe doped with high pressures (up to 80 atm) of dinitrogen gas, have been used at room temperature to photochemically synthesize transition metal dinitrogen complexes [42]. However, the use of time-resolved spectroscopic techniques, in particular TRIR spectroscopy, enables the rate

Table 2
Second-order rate constants, k_{N_2} for the reaction of various photogenerated transition metal intermediates with N_2 to generate the corresponding dinitrogen complexes, in solution at room temperature

Precursor	Solvent	Reacting intermediate	Product	Technique	k_{N_2} (M^{-1} s^{-1})	Ref.
$Cr(CO)_6$	C_7F_{14}	$Cr(CO)_5$	$Cr(CO)_5(N_2)$	UV–vis	$(9.6 \pm 2.9) \times 10^8$[a]	[43]
$Mo(CO)_6$	C_7F_{14}	$Mo(CO)_5$	$Mo(CO)_5(N_2)$	UV–vis	$(7.2 \pm 2.2) \times 10^8$[a]	[43]
$Cr(CO)_6$	Cyclohexane	$Cr(CO)_5(C_6H_{12})$	$Cr(CO)_5(N_2)$	TRIR	$\leq 2.2 \times 10^6$	[30]
$Cr(CO)_6$	*n*-Heptane	$Cr(CO)_5(C_7H_{16})$	$Cr(CO)_5(N_2)$	TRIR	6.2×10^6	[49]
$Mo(CO)_6$	*n*-Heptane	$Mo(CO)_5(C_7H_{16})$	$Mo(CO)_5(N_2)$	TRIR	6.0×10^6	[49]
$W(CO)_6$	*n*-Heptane	$W(CO)_5(C_7H_{16})$	$W(CO)_5(N_2)$	TRIR	5.4×10^5	[49]
$(NBD)Mo(CO)_4$	*n*-Heptane	*fac*-$(NBD)Mo(CO)_3(C_7H_{16})$	*fac*-$(NBD)Mo(CO)_3(N_2)$	TRIR	3.0×10^7	[49]
$(NBD)Mo(CO)_4$	*n*-Heptane	*mer*-$(NBD)Mo(CO)_3(C_7H_{16})$	*mer*-$(NBD)Mo(CO)_3(N_2)$	TRIR	9.0×10^5	[49]
$CpMn(CO)_3$	Cyclohexane	$CpMn(CO)_2(C_6H_{12})$	$CpMn(CO)_2(N_2)$	UV–vis	$(3.7 \pm 0.4) \times 10^5$	[16]
$CpMn(CO)_3$	*n*-Heptane	$CpMn(CO)_2(C_7H_{16})$	$CpMn(CO)_2(N_2)$	TRIR	$(4.7 \pm 0.5) \times 10^5$	[53]
$Cp^*Mn(CO)_3$	*n*-Heptane	$Cp^*Mn(CO)_2(C_7H_{16})$	$Cp^*Mn(CO)_2(N_2)$	TRIR	$(1.1 \pm 0.1) \times 10^6$	[53]
$Cp^{Et}Mn(CO)_3$	*n*-Heptane	$Cp^{Et}Mn(CO)_2(C_7H_{16})$	$Cp^{Et}Mn(CO)_2(N_2)$	TRIR	$(2.6 \pm 0.3) \times 10^6$	[53]
$CpV(CO)_4$	*n*-Heptane	$CpV(CO)_3(C_7H_{16})$	$CpV(CO)_3(N_2)$	TRIR	1.5×10^8	[55]
$Cp^*V(CO)_4$	*n*-Heptane	$Cp^*V(CO)_3(C_7H_{16})$	$Cp^*V(CO)_3(N_2)$	TRIR	3.6×10^8	[55]
$CpNb(CO)_4$	*n*-Heptane	$CpNb(CO)_3(C_7H_{16})$	$CpNb(CO)_3(N_2)$	TRIR	4.9×10^6	[55]
$CpTa(CO)_4$	*n*-Heptane	$CpTa(CO)_3(C_7H_{16})$	$CpTa(CO)_3(N_2)$	TRIR	2.9×10^6	[55]
$V(CO)_6$	*n*-Heptane	$V(CO)_5(C_7H_{16})$	$V(CO)_5(N_2)$	TRIR	2.5×10^7[b]	[55]
$CpNb(CO)_4$	*n*-Heptane	$CpNb(CO)_3(C_7H_{16})$	$CpNb(CO)_3(N_2)$	TRIR	2.2×10^6	[56]
$CpTa(CO)_4$	*n*-Heptane	$CpTa(CO)_3(C_7H_{16})$	$CpTa(CO)_3(N_2)$	TRIR	1.3×10^6	[56]
$(\eta^5\text{-}C_9H_7)Nb(CO)_4$	*n*-Heptane	$(\eta^5\text{-}C_9H_7)Nb(CO)_3(C_7H_{16})$	$(\eta^5\text{-}C_9H_7)Nb(CO)_3(N_2)$	TRIR	1.9×10^7	[56]
$(\eta^5\text{-}C_9H_7)Ta(CO)_4$	*n*-Heptane	$(\eta^5\text{-}C_9H_7)Ta(CO)_3(C_7H_{16})$	$(\eta^5\text{-}C_9H_7)Ta(CO)_3(N_2)$	TRIR	1.1×10^7	[56]
$[P(CH_2CH_2PPh_2)_3]Ru(H)_2$	Cyclohexane	$[P(CH_2CH_2PPh_2)_3]Ru$	$[P(CH_2CH_2PPh_2)_3]Ru(N_2)$	UV–vis	$(7.5 \pm 1.8) \times 10^5$	[57]
$[P(CH_2CH_2PPh_2)_3]Os(H)_2$	Cyclohexane	$[P(CH_2CH_2PPh_2)_3]Os$	$[P(CH_2CH_2PPh_2)_3]Os(N_2)$	UV–vis	2.2×10^6	[57]
mer,*trans*-$W(CO)_3(PCy_3)_2(N_2)$	Toluene	*mer*,*trans*-$W(CO)_3(PCy_3)_2$	*mer*,*trans*-$W(CO)_3(PCy_3)_2(N_2)$	UV–vis	$(3.0 \pm 0.2) \times 10^5$	[c]

[a] We have recalculated these values using the author's original data. See main text for details.
[b] The average of the two values that were reported.
[c] This work. C_7F_{14}: perfluoromethylcyclohexane; NBD: norbornadiene; Cp: $(\eta^5\text{-}C_5H_5)$; Cp^*: $(\eta^5\text{-}C_5Me_5)$; Cp^{Et}: $(\eta^5\text{-}C_5Et_5)$; $(\eta^5\text{-}C_9H_7)$: indenyl; Cy: cyclohexyl; TRIR: time-resolved infrared spectroscopy; UV–vis: UV–vis flash photolysis.

constant for the binding of dinitrogen to transition metal centers and the reactivity of the resulting dinitrogen complexes to be directly measured in solution at room temperature. This is important, since it is vital that we fully understand the nature of the reactivity of transition metal centers toward dinitrogen in solution, under the ambient conditions that would potentially exist in a catalytic nitrogen fixation process. Therefore, in this paper we do not intend to review the extensive and elegant work on the formation and identification of dinitrogen complexes at cryogenic temperatures or in supercritical fluids, and instead will focus on time-resolved spectroscopic studies in room temperature solution.

In an early UV–vis laser flash photolysis study [43] on $M(CO)_6$ (M = Cr and Mo) in room temperature perfluoromethylcyclohexane solution saturated with dinitrogen, Kelly and co-workers were able to monitor the growth of a transient species that they assigned to $M(CO)_5(N_2)$ from its absorption maximum at 370 nm (for M = Cr), consistent with previous low temperature matrix isolation data [39]. The use of a perfluorinated solvent was innovative since unlike conventional organic solvents, which generally act as weakly bound "token" ligands at unsaturated metal centers [10], the perfluorinated solvent molecules can be considered, at best, to be only extremely weakly coordinating [44] with respect to the unsaturated $M(CO)_5$ fragments that are generated upon photolysis of $M(CO)_6$. Thus, the binding rates of N_2 to the almost "naked" $M(CO)_5$ fragments could be directly measured without any significant competition from solvent molecules. From their data, the second order rate constants for the binding of dinitrogen to $M(CO)_5$ (see Table 2) are calculated to be $(9.6 \pm 2.9) \times 10^8$ M^{-1} s^{-1} (for M = Cr) and $(7.2 \pm 2.2) \times 10^8$ M^{-1} s^{-1} (for M = Mo),[1] which, as expected for reaction with an almost unsaturated 16-electron fragment, are approaching the diffusion-controlled limit for perfluoromethylcyclohexane (4.2×10^9 M^{-1} s^{-1} at 25 °C) [46].

Despite the fact that Kelly and co-workers had already monitored the reaction of $M(CO)_5$ (M = Cr and Mo) with N_2 by UV–vis flash photolysis, the first truly definitive identification of a transition metal–dinitrogen complex in room temperature solution was by Grevels and co-workers in their TRIR study of $Cr(CO)_6$ in dinitrogen saturated cyclohexane [30]. Flash photolysis of the solution initially generated the solvated species, $Cr(CO)_5$(cyclohexane) within the instrument response time (5 μs). This was found to decay exponentially ($k_{obs} = 1.8 \times 10^4$ s^{-1}) concurrent with the growth of five new IR bands, which were assigned to the $Cr(CO)_5(N_2)$ complex. Three of these bands (at 2086, 1976 and 1966 cm^{-1}) are due to the ν(CO) vibrations of $Cr(CO)_5(N_2)$. However, the definitive identification of $Cr(CO)_5(N_2)$ came from the observation

[1] We have recalculated the rate constants from the authors' reported data using a concentration of 1.67×10^{-2} M per atm for N_2 in perfluoromethylcyclohexane [45], since it appears that the authors erroneously used a concentration of 1.2×10^{-2} M in their calculations.

of its ν(NN) band at 2240 cm^{-1} and a ^{13}CO satellite ν(CO) IR band at 1946 cm^{-1}. Based on the pressure of N_2 gas that was used to saturate their solutions and the solubility of N_2 in cyclohexane [45], an upper limit can be estimated from their data for the second-order rate constant for reaction of $Cr(CO)_5$(cyclohexane) with N_2 in cyclohexane solution, $k_{N_2} \leq 2.2 \times 10^6\ M^{-1}\ s^{-1}$ (see Table 2). This result clearly demonstrates the strong influence that the nature of the solvent has on the binding rate of N_2 to a transition metal center in solution, since the formation of $Cr(CO)_5(N_2)$ in the more coordinating cyclohexane is slower than in the virtually non-coordinating perfluoromethylcyclohexane [43] by a factor of at least 500. The activation barrier in cyclohexane will involve the dissociation of the weakly bound solvent molecule as shown below,

$$Cr(CO)_5(C_6H_{12}) \rightarrow Cr(CO)_5 + C_6H_{12}$$

This has important implications for controlling the rates and mechanisms of individual steps in transition metal catalyzed nitrogen fixation cycles via the donating ability of the chosen solvent. $Cr(CO)_5(N_2)$ was found to decay to an unidentified species via first-order kinetics with a lifetime of ~0.6 s. The rate constants for the formation and decay of $Cr(CO)_5(N_2)$ and the related dihydrogen complex, $Cr(CO)_5(H_2)$ [47] in cyclohexane are very similar, suggesting that these two species have similar stabilities in room temperature solution.

Poliakoff and co-workers later made elegant use of IR spectroscopy to investigate the photocatalytic mechanism of the hydrogenation of norbornadiene (NBD) by group 6 metal carbonyls in *n*-heptane solution [48,49]. During the course of their investigations they used TRIR spectroscopy to probe the reactivity of $M(CO)_5$(*n*-heptane) (M = Cr, Mo and W) and *fac*- and *mer*-(NBD)$Mo(CO)_3$(*n*-heptane) with N_2. XeCl excimer laser flash photolysis (308 nm) of $M(CO)_6$ or (NBD)$Mo(CO)_4$ in *n*-heptane generated $M(CO)_5$(*n*-heptane) or a mixture of *fac*- and *mer*-(NBD)$Mo(CO)_3$(*n*-heptane), respectively as the primary photoproducts, identified by TRIR. In solutions that were saturated under 1 atm of N_2, they monitored the pseudo-first-order decays of the ν(CO) bands of the *n*-heptane complexes and the growths of the ν(CO) bands of the dinitrogen complexes that were formed by reaction with N_2. Experiments were also conducted under argon and the data were used to calculate the second-order rate constants for the reactions of the various *n*-heptane solvated complexes with N_2 (see Table 2). It can be seen that $Cr(CO)_5$(*n*-heptane) reacts at least 2.8 times faster with N_2 than the corresponding $Cr(CO)_5$(cyclohexane) species. It is tempting to conclude that this difference in reactivity is simply a result of *n*-heptane interacting more weakly with the Cr center than cyclohexane. However, recent studies [50–52] have shown that the difference in reactivity between cyclic- and linear-alkane solvated complexes toward small molecules can be explained by changes in the entropy of activation, $\Delta S^{\ddagger}$ of these reactions and not by variations in the interaction energy between the unsaturated metal center and solvent. Thus, the increase in the $\Delta S^{\ddagger}$ term upon displacement of the coordinated alkane by a small molecule, such as N_2, is more pronounced for longer chain linear alkanes than for shorter chain and cyclic alkanes, leading to enhanced rate constants. Another interesting result was that *fac*-(NBD)$Mo(CO)_3$(*n*-heptane) reacts with N_2 ca. 33 times faster than *mer*-(NBD)$Mo(CO)_3$(*n*-heptane). This was concluded to be due to steric and electronic factors in the *fac* configuration causing a labilization of the coordinated solvent ligand.

Room temperature solution studies have not been restricted to the group 6 carbonyls. UV flash photolysis of $CpMn(CO)_3$ in cyclohexane generated $CpMn(CO)_2$(cyclohexane) as the primary photoproduct, which was detected by its broad absorption maximum at ca. 580 nm [16]. Support for this assignment also came from the positions of the two transient ν(CO) bands observed in the corresponding TRIR spectrum recorded in *n*-heptane solution. The second-order rate constant for the subsequent reaction of the cyclohexane solvated species with added N_2, to form $CpMn(CO)_2(N_2)$ was measured by UV–vis flash photolysis to be $(3.7 \pm 0.4) \times 10^5\ M^{-1}\ s^{-1}$. A subsequent, more detailed TRIR investigation into this type of reaction in *n*-heptane solution using the series of complexes, (η^5-C_5R_5)$Mn(CO)_3$ (R = H, Me and Et) was performed [53]. The second-order rate constants for reaction of N_2 with the photogenerated species, (η^5-C_5R_5)$Mn(CO)_2$(*n*-heptane) to form (η^5-C_5R_5)$Mn(CO)_2(N_2)$ were calculated from the pseudo-first-order rates of decay of the transient ν(CO) bands in the absence and presence of N_2. These binding rates were found to be $(0.47 \pm 0.05) \times 10^6\ M^{-1}\ s^{-1}$ (for R = H), $(1.1 \pm 0.1) \times 10^6\ M^{-1}\ s^{-1}$ (for R = Me) and $(2.6 \pm 0.3) \times 10^6\ M^{-1}\ s^{-1}$ (for R = Et), see Table 2. Due to the fact that the electron density at the metal center is lower for R = H than for R = Me and Et (in which it is approximately the same) and the fact that the steric bulk of the cyclopentadienyl ligands steadily increases in the order, R = H < Me < Et, the origin of the effect on the dinitrogen binding rate constant (and also the rate constants observed for reaction with other small molecules) was concluded to be steric rather than electronic, because electronic factors should be similar for R = Me and Et. The precise nature of the steric influence could not be definitively determined. However, it was suggested that since steric interactions with small incoming molecules, such as N_2, H_2 and CO, are likely to be small, the major steric effect is probably a gradual weakening of the Mn. . .(*n*-heptane) interaction as the cyclopentadienyl ligand is substituted with more and more bulky substituents. This would make it easier to displace the coordinated solvent molecule and thus increase the rate of dinitrogen binding in the order, R = H < Me < Et. This was an important result, since it shows that substituents some distance from a metal center can strongly influence the rate of reaction at that center. Therefore, even minor modifications of peripheral ligands could have large effects on competitive reaction steps in catalytic nitrogen fixation cycles.

Group 5 metal–dinitrogen complexes have also received considerable attention in room temperature TRIR investigations. Following an initial report [54] in which TRIR was used to monitor the photochemical generation of $CpV(CO)_3(N_2)$ from $CpV(CO)_4$ in *n*-heptane solution saturated under 1.5 atm N_2, a subsequent, much more detailed and thorough, investigation [55] used IR spectroscopy to study the photochemical reactions of N_2 (and also H_2) with $CpM(CO)_4$ and $Cp^*V(CO)_4$ (M = V, Nb

and Ta; $Cp^* = \eta^5$-C_5Me_5) both in liquid xenon at −80 °C (using FTIR) and in *n*-heptane at room temperature (using TRIR). The TRIR experiments were performed in the absence of N_2 (under argon) and in the presence of N_2, by monitoring the first-order decay of one of the ν(CO) bands of $Cp'M(CO)_3$(*n*-heptane) ($Cp' = Cp$ or Cp^*), which was formed immediately after the laser flash, and the growth of one of the ν(CO) bands of $Cp'M(CO)_3(N_2)$. These pseudo-first order rates were then used to calculate the second-order rate constants for reaction of $Cp'M(CO)_3$(*n*-heptane) with N_2 to generate $Cp'M(CO)_3(N_2)$ (see Table 2). Note that the V complexes are up to 100 times more reactive toward N_2 than the Nb and Ta complexes and that the $Cp'V(CO)_3$(*n*-heptane) species are ca. 320 times more reactive than $Cp'Mn(CO)_2$(*n*-heptane) toward N_2 under similar conditions. $CpV(CO)_3(N_2)$ was found not to be stable in solution at room temperature, reacting slowly with photodissociated CO to regenerate $CpV(CO)_4$. However, the investigators clearly demonstrated that its lifetime could be extended by increasing the pressure of N_2 over the solution. Indeed, the lifetime was lengthened from 1 to 4 ms upon increasing the pressure of N_2 from 0.5 to 2 atm. The Nb and Ta dinitrogen complexes were significantly longer lived and therefore their decay could not be monitored accurately with the TRIR apparatus. The photochemical reaction of $V(CO)_6$ with N_2 was also investigated by TRIR in *n*-heptane solution in order to compare the behavior of d^5 vanadium with the d^4 complexes. The binding rate constant of N_2 to the photochemically generated $V(CO)_5$(*n*-heptane) complex to generate $V(CO)_5(N_2)$ was ca. 10 times lower than that for $CpV(CO)_3$(*n*-heptane) (see Table 2), indicating the much lower reactivity of $V(CO)_5$(*n*-heptane) toward N_2. However, $V(CO)_5(N_2)$ was much less thermally stable in solution ($\tau = 0.2$ ms) than $CpV(CO)_3(N_2)$ ($\tau = 4$ ms) under 2 atm of N_2.

The group 5 studies were recently extended in the same laboratory, using a combination of two different TRIR techniques; conventional diode laser-based point-by-point TRIR and step-scan FTIR spectroscopy [56]. The photochemical reactions of $CpM(CO)_4$ and (η^5-C_9H_7)$M(CO)_4$ (M = Nb and Ta; η^5-C_9H_7 = indenyl) with N_2 and other small molecules were monitored in *n*-heptane solution. Second-order rate constants for reaction of the various photochemically generated tricarbonyl *n*-heptane solvated species with N_2 were determined more accurately than in previous studies by repeating the experiments over a range of different N_2 concentrations and plotting graphs of observed decay rates versus [N_2] to obtain the second-order rates from the slopes (see Table 2). The rate constants measured for $CpM(CO)_3$(*n*-heptane) are slightly lower than the previously published values [55], presumably due to the more accurate method of their determination. Interestingly, the indenyl complexes were found to be approximately one order of magnitude more reactive toward N_2 than the corresponding Cp complexes. Furthermore, the resulting indenyl–dinitrogen complexes were 20–26 times less stable than the corresponding Cp-dinitrogen species. The difference in rate constants and stabilities of the indenyl complexes compared to the Cp complexes was concluded to be a subtle combination of steric effects and decay of the indenyl complexes via a ring-slipped intermediate species.

The formation of group 8 dinitrogen complexes has also been studied in solution. UV laser flash photolysis of the dihydride precursors, $M(PP_3)H_2$ (M = Ru and Os; $PP_3 = P(CH_2CH_2PPh_2)_3$) in cyclohexane solution resulted in the elimination of dihydrogen and the instantaneous formation of the transient species, $M(PP_3)$, which exhibited single absorption maxima at 395 nm (M = Ru) and 390 nm (M = Os), respectively [57]. Although they could not eliminate the possibility of solvent coordination to these unsaturated transient intermediates, the investigators concluded that instead, an agostic interaction at the vacant coordination site via a C–H bond of one of the phenyl groups offered the most satisfactory explanation of all of their experimental observations. Thus, the reaction of these agostically stabilized d^8 $M(PP_3)$ transients with N_2 was monitored by flash photolysis in nitrogen saturated cyclohexane solution. Second-order rate constants for the binding of N_2 to generate $M(PP_3)(N_2)$ were found to be $(7.5 \pm 1.8) \times 10^5\ M^{-1}\ s^{-1}$ (M = Ru) and $2.2 \times 10^6\ M^{-1}\ s^{-1}$ (M = Os), respectively (see Table 2).

2. Rate of binding of dinitrogen to *mer*,*trans*-$W(CO)_3(PCy_3)_2$

2.1. Introduction

In 1983, Kubas and co-workers isolated the first example of a molecular dihydrogen complex, *mer*,*trans*-$W(CO)_3(P^iPr_3)_2(\eta^2$-$H_2)$ (^{i}Pr = isopropyl) [58–61]. This was a remarkable discovery since it had previously been believed that molecules containing strong σ bonds, such as H–H in H_2 and C–H in hydrocarbons, were incapable of forming stable bonds with a metal center. The bonding in M–(η^2-H_2) is non-classical and similar to that of three-center, two-electron bonding in carbocations. It involves a simple donation of electrons from the σ-bonding electron pair of the side-on bound H_2 ligand to a vacant orbital of the metal. However, the metal center further stabilizes the H_2 bonding by backdonation from a filled d orbital to the σ^* orbital of the H–H bond. The family of $W(CO)_3(PR_3)_2$ and $W(CO)_3(PR_3)_2(H_2)$ complexes are now often referred to as the 'Kubas complexes'. The deep purple $W(CO)_3(PR_3)_2$ complexes readily react with N_2 to produce stable, yellow dinitrogen complexes [62]. In the case of $W(CO)_3(PCy_3)_2$ (Cy = cyclohexyl), the product was identified as the terminally bound dinitrogen complex, $W(CO)_3(PCy_3)_2(N_2)$, based on the observation of its ν(NN) stretching frequency at 2120 cm^{-1} in the solid state [62]. However, in the case of $W(CO)_3(P^iPr_3)_2$, the N_2 bridged, $W(CO)_3(P^iPr_3)_2$–N≡N–$W(CO)_3(P^iPr_3)_2$ species, with ν(NN) at 1939 cm^{-1} and mixed ν(NN)/ν(CO) at 1996 cm^{-1}, was isolated as a product of the reaction and the structure was confirmed by a single crystal X-ray diffraction study [63].

Hoff's group elegantly employed stopped-flow kinetics, measuring the indirect substitution reaction of **W**–L (**W** = $W(CO)_3(PCy_3)_2$, L = H_2 and N_2) with pyridine in toluene to evaluate $k_{f(H_2)}$ and $k_{f(N_2)}$ to be $(2.2 \pm 0.3) \times 10^6$ and $(5.0 \pm 1.0) \times 10^5\ M^{-1}\ s^{-1}$, respectively (Eq. (1)), on the basis of the reaction mechanism outlined in Eqs. (1)–(4), using $k_{f(py)} = 8.0 \times 10^5\ M^{-1}\ s^{-1}$ [64]. Since the value of $k_{f(py)}$ for

Eq. (2) is too fast to measure on a stopped-flow apparatus, they calculated it from the competition reaction (Eq. (4)) with $P(OMe)_3$, whose reaction rate (Eq. (3)) can be accurately determined. Calorimetric data were also determined for reaction 1. The enthalpies for the addition of L to **W** were found to be, 13 (L = N_2), 10 (L = H_2), 15 (L = CH_3CN), 19 (L = py), 26 (L = $P(OMe)_3$) and 30 kcal mol^{-1} (L = CO) [65,66].

$$\mathbf{W}\text{–L} \underset{k_f}{\overset{k_r}{\rightleftharpoons}} \mathbf{W} + \text{L} \quad (1)$$

$$\mathbf{W} + \text{py} \xrightarrow{k_{f(py)}} \mathbf{W}\text{–py} \quad (2)$$

$$\mathbf{W} + \text{P(OMe)}_3 \xrightarrow{k_{f(P(OMe)_3)}} \mathbf{W}\text{–P(OMe)}_3 \quad (3)$$

$$\mathbf{W}\text{–py} + \text{P(OMe)}_3 \rightarrow \mathbf{W}\text{–P(OMe)}_3 + \text{py} \quad (4)$$

W is formally a 16-electron species, however an agostic interaction with the tungsten center from a C–H bond of a cyclohexyl group on one of the phosphine ligands, stabilizes the electronic unsaturation to such a degree that **W** is stable in solution at room temperature. The agostic interaction is clearly seen in the X-ray structure (2.27 Å for the W–H distance) [62] and its energy is estimated to be 10 ± 6 kcal mol^{-1} [65]. In our study, a combination of nanosecond UV–vis flash photolysis and time-resolved step-scan FTIR (s^2-FTIR) spectroscopy was used to spectroscopically characterize the photoproduct, **W** and to directly measure the rate constant for binding of N_2 to **W** to reform **W**–N_2, following laser flash photolysis of **W**–N_2. When a toluene or *n*-hexane solution containing **W**–N_2 and a known amount of additional N_2 was irradiated with a 355 nm laser pulse, **W**–N_2 bond dissociation took place to form **W**. Subsequently, clean regeneration of **W**–N_2 was observed using time-resolved UV–vis and s^2-FTIR spectroscopy. In addition, we performed density functional theory (DFT) calculations at the B3LYP level of theory on **W′** and **W′**–N_2 (**W′** = $W(CO)_3(PH_3)_2$) in an effort to understand the UV–vis and s^2-FTIR results.

2.2. Experimental

mer,*trans*-$W(CO)_3(PCy_3)_2$ (**W**) was prepared as previously described [62] and characterized by NMR, UV–vis and FTIR spectroscopy. Toluene and *n*-hexane were distilled over sodium benzophenone ketyl and CaH_2, respectively under an Ar atmosphere and stored inside a glove box. Ultra high purity N_2 and Ar (Praxair) were used without further purification. UV–vis spectra were measured on a Hewlett-Packard 8452A diode array spectrophotometer. Toluene solutions containing **W** were prepared in home-built glassware equipped with an optical cell, inside a glove box. After the UV–vis spectrum was measured, a known amount of dinitrogen gas was added using a vacuum line equipped with a pressure gauge in order to generate **W**–N_2. The solubilities of N_2 in toluene and *n*-hexane were calculated from previously published data [45]. The following values were used; $[N_2] = 5.39$ and 10.7 mM in toluene and *n*-hexane, respectively, at a N_2 partial pressure of 1 atm.

UV–vis flash photolysis experiments were conducted using an apparatus described previously [67,68], with excitation being provided by the third harmonic (355 nm, ∼5 ns, ∼20 mJ/pulse) of a Continuum Surelite I-10 Nd:YAG laser. These experiments were performed in toluene at 25 °C under 1 atm of Ar or under a known pressure of N_2.

FTIR spectra were recorded on a Bruker IFS 66/S spectrometer. Time-resolved step-scan FTIR (s^2-FTIR) experiments were performed by operating the FTIR spectrometer in step-scan mode and using the third harmonic of the Nd:YAG laser to excite the sample at a repetition rate of 5 Hz (Laser master/FTIR slave). A 1 mm photovoltaic HgCdTe infrared detector equipped with a 20 MHz pre-amplifier (Kolmar, KMPV11-1-LJ2/239) was used in these experiments. Due to intense absorptions of toluene in the metal carbonyl infrared region, the s^2-FTIR experiments were performed in *n*-hexane solution. The dry, degassed purple *n*-hexane solutions of **W** were saturated with a known pressure of dinitrogen in order to generate **W**–N_2, which was a pale yellow color. The solutions were handled in an air-sensitive manner and flowed cyclically through an air-tight, home-built flow system consisting of 1/8 in. o.d. stainless steel tubing, a sample reservoir vessel, a CaF_2 IR flow cell (Harrick Scientific Products, DLC-S25) and a recirculating gear pump (Micropump, GA-V23). Complete details of the s^2-FTIR apparatus will be provided in an upcoming paper [69].

The Gaussian 03 package of programs [70] was employed for DFT calculations on the model complexes, *mer*,*trans*-$W(CO)_3(PH_3)_2$ (**W′**) and *mer*,*trans*-$W(CO)_3(PH_3)_2(N_2)$ (**W′**–N_2) in the gas phase, using the Hay-Wadt VDZ ($n+1$) ECP (LANL2DZ ECP) basis set for W [71–73] and the 6-31G** basis set for H, C, N and O [74–76]. Geometry optimizations were performed using the B3LYP method [77–79]. Time-dependent B3LYP DFT calculations and frequency analysis were carried out in order to predict the UV–vis and FTIR spectra, respectively. In our experience [80], B3LYP DFT calculations on second- and third-row transition metal complexes yield binding energies that are accurate to within 4–6 kcal mol^{-1} compared with experimental data and MP2 calculations.

2.3. Results and discussion

2.3.1. UV–vis and flash photolysis

UV–vis spectra of **W** and **W**–N_2 in toluene are shown in Fig. 1. When 760 Torr of N_2 was added to a purple solution of **W**, the 566 nm absorption of **W** completely disappeared due to the high stability of the **W**–N_2 species being formed (Eq. (5)). Upon removal of N_2 by freeze–pump–thaw cycles, from the solution containing the **W**–N_2 species, the original **W** spectrum was cleanly reproduced.

$$\mathbf{W} + N_2 \underset{k_r}{\overset{k_f}{\rightleftharpoons}} \mathbf{W}\text{-}N_2 \quad (5)$$

The transient absorption spectrum of the short-lived species observed by flash photolysis, 2 μs after excitation of a toluene solution containing **W**–N_2, indicates that this transient species is **W**, by comparison with the UV–vis spectra shown in Fig. 1. Clean reformation of **W**–N_2 was observed in less than a few ms. The observed pseudo-first order rate constant for the reformation

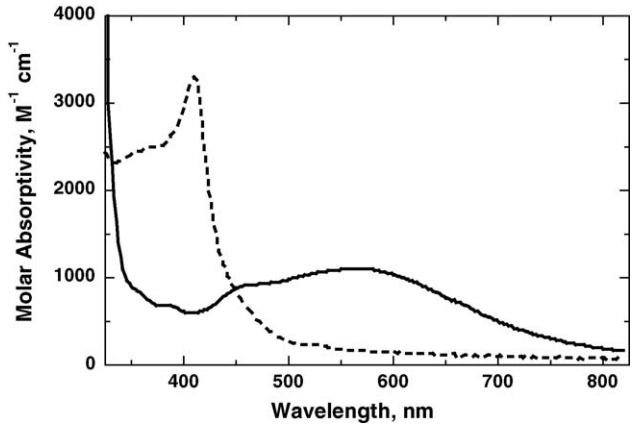

Fig. 1. UV–vis spectra of **W** (solid line) and **W**–N_2 (dashed line) in toluene.

process is described by Eq. (6). The forward dinitrogen binding rate constant ($k_f = (3.0 \pm 0.2) \times 10^5\ M^{-1}\ s^{-1}$) and reverse rate constant ($k_r = 100 \pm 10\ s^{-1}$) were determined from the slope and intercept, respectively, of the graph shown in Fig. 2, which was generated by repeating the experiment over a range of N_2 pressures. The equilibrium constant, $K_{N_2} = (3.0 \pm 0.5) \times 10^3\ M^{-1}$, for the formation of the dinitrogen complex was estimated using Eq. (7). Our second-order rate constant, $k_{f(N_2)} = (3.0 \pm 0.2) \times 10^5\ M^{-1}\ s^{-1}$, is similar to that ($k_{f(N_2)} = (5.0 \pm 1.0) \times 10^5\ M^{-1}\ s^{-1}$) obtained by Hoff using stopped-flow kinetics of the indirect substitution reaction of **W**–N_2 with pyridine [64]. However, the equilibrium constant, $K_{N_2} = (3.0 \pm 0.5) \times 10^3\ M^{-1}$, determined in the present study is smaller than that ($K_{N_2} = 6.7 \times 10^3\ M^{-1}$) which we have calculated, according to Eq. (7), from the k_f and k_r rates reported by Hoff and co-workers in their stopped–flow study [64]. While their K_{N_2} is ca. ×2 larger than ours, considering the large experimental errors involved in both techniques, the values are actually in reasonable agreement

$$k_{obs} = k_f[N_2] + k_r \quad (6)$$

$$K_{N_2} = k_f/k_r \quad (7)$$

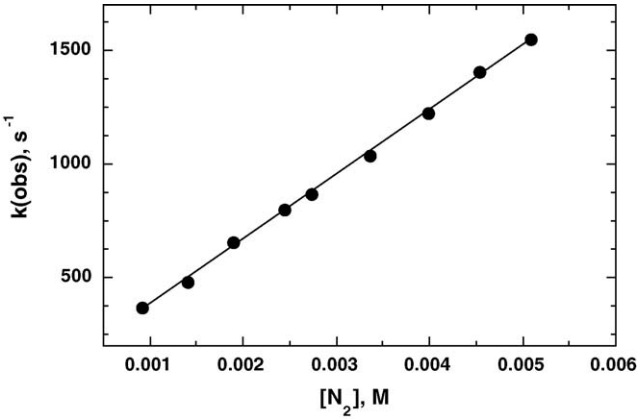

Fig. 2. Plot of observed rate constants for the formation of **W**–N_2 as a function of N_2 concentration in toluene at 25 °C. [N_2] = 5.39 mM/atm at 25 °C [45]. The data were obtained from single exponential fits to the decay of **W** (at 600 nm) that was generated following flash photolysis of **W**–N_2.

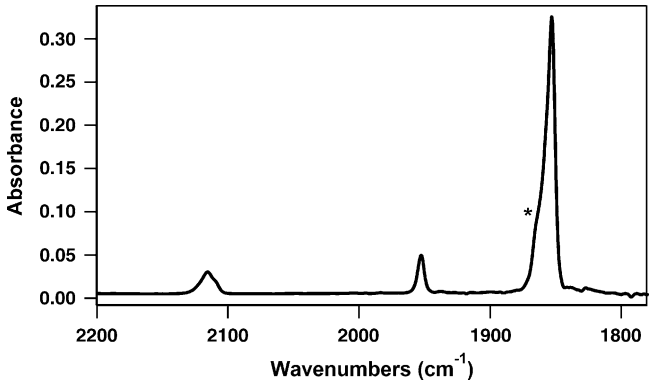

Fig. 3. FTIR spectrum of **W**–N_2 in *n*-hexane solution under 1.8 atm N_2 at 23 °C. *: Minor *trans*-$W(CO)_4(PCy_3)_2$ impurity. See text for details.

2.3.2. Time-resolved step-scan FTIR

Fig. 3 shows the FTIR spectrum of **W**–N_2 in *n*-hexane, saturated with 1.8 atm of N_2. Multi-peak curve-fitting reveals that there are two overlapping bands at 2117 and 2113 cm^{-1} in the ν(NN) region (see DFT section later) and that there are three ν(CO) bands, two of which are heavily overlapped at 1857 and 1853 cm^{-1}, while the third appears at 1953 cm^{-1}. A shoulder due to minor contamination by *trans*-$W(CO)_4(PCy_3)_2$ is also present at 1865 cm^{-1}. Solutions of **W** and **W**–L (L = N_2, H_2, etc.) are known to slowly decompose via disproportionation and/or minor air-oxidation into the extremely stable *trans*-$W(CO)_4(PCy_3)_2$ and therefore their IR spectra often contain a small ν(CO) band due to *trans*-$W(CO)_4(PCy_3)_2$ impurity [62,81]. We have found that the rate of this decomposition appears to be greater in *n*-hexane than in toluene and therefore the *trans*-$W(CO)_4(PCy_3)_2$ peak sometimes increased slightly in intensity during the course of the s^2-FTIR experiments.

A series of s^2-FTIR spectra recorded at 5 μs intervals following 355 nm excitation of this solution are shown in Fig. 4 as a 3D plot. On this timescale, an instantaneous depletion of the ν(NN) and ν(CO) bands of **W**–N_2 is observed, accompanied by the formation of two new transient ν(CO) absorptions at 1837 and 1819 cm^{-1}. These are assigned to **W**, by comparison with

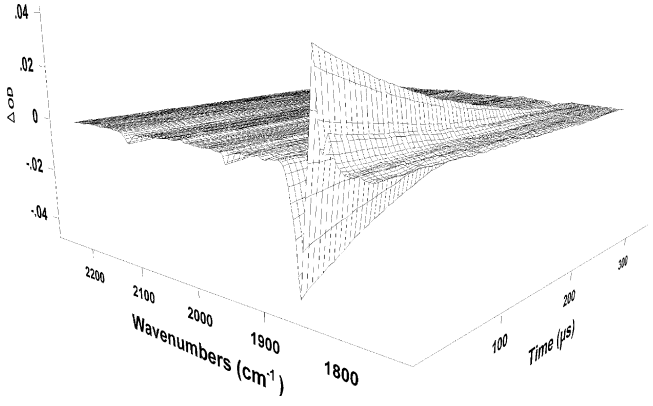

Fig. 4. Step-scan FTIR spectra recorded at 5 μs intervals following 355 nm excitation of **W**–N_2 in *n*-hexane saturated with 1.8 atm of N_2 at 23 °C. Negative bands are due to the depletion and subsequent recovery of **W**–N_2 and positive bands are assigned to the formation and subsequent decay of **W** as it regenerates **W**–N_2 by reaction with N_2.

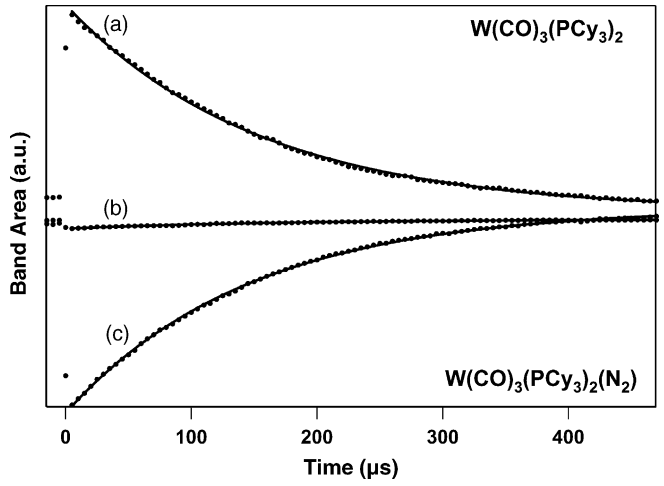

Fig. 5. TRIR kinetic traces from the **W**–N_2 s^2-FTIR experiment, obtained from the areas of the bands at (a) 1837 cm^{-1} (ν(CO) of **W**), (b) 2115 cm^{-1} (ν(NN) of **W**–N_2) and (c) 1853 cm^{-1} (ν(CO) of **W**–N_2). Dots: experimental data points; curves: exponential fits to the data.

the FTIR spectrum of **W** that we had previously recorded in *n*-hexane under argon. In the s^2-FTIR experiment, **W** is formed by photo-ejection of the N_2 ligand from **W**–N_2, as was also observed in the UV–vis flash photolysis experiments. The third, much weaker band of **W**, which should appear at 1949 cm^{-1} is too close to the 1953 cm^{-1} depletion to be clearly observed at the spectral resolution of this experiment.

The transient ν(CO) bands were subsequently observed to decay exponentially at an identical rate, within experimental error, ($k_{obs} = 6530 \pm 650\ s^{-1}$) to the recovery ($k_{obs} = 6840 \pm 680$ and $5730 \pm 570\ s^{-1}$, respectively) of the ν(CO) and ν(NN) bands of **W**–N_2 (Fig. 5), thus indicating a clean reformation of the **W**–N_2 complex by reaction, under pseudo-first order conditions, of **W** with the excess N_2 present in solution. In contrast to the UV–vis flash photolysis experiments, the spectra in Fig. 4 demonstrate the power of TRIR spectroscopy to definitively identify transient species from their well-defined and narrow IR absorption bands. Furthermore, the s^2-FTIR spectra clearly reveal that **W** and **W**–N_2 were the only carbonyl containing products formed during the photoreaction i.e. no secondary photoproducts were observed.

Despite the fact that it was necessary to perform the s^2-FTIR experiments in *n*-hexane rather than in toluene (due to intense IR absorption bands of toluene in the ν(CO) region), the pseudo-first-order lifetimes of **W** and **W**–N_2 observed by s^2-FTIR are in good agreement, within experimental error, with the pseudo-first order lifetime predicted from Eq. (6) using the k_f and k_r rate constants that were determined from our UV–vis flash photolysis experiments in toluene, and the concentration of N_2 in *n*-hexane at a N_2 partial pressure of 1.8 atm [45].

2.3.3. Density functional theory calculations

We also performed gas-phase DFT calculations at the B3LYP level of theory on the model complexes, *mer*,*trans*-$W(CO)_3(PH_3)_2(N_2)$ (**W′**–N_2) (for both end-on and side-on bound dinitrogen) and *mer*,*trans*-$W(CO)_3(PH_3)_2$ (**W′**). These calculations were initially performed in an effort to confirm our observation of three ν(CO) bands in the IR spectrum of **W**–N_2, since only two bands had previously been reported in the literature [62]. The DFT calculated **W′**–N_2 bond energy, bond distances for **W′** and **W′**–N_2, and DFT and experimental ν(CO) and ν(NN) IR data are summarized in Table 3. The bond energy quoted here is not corrected for basis set superposition error (BSSE). However, a counterpoise calculation on the optimized geometry of the N_2 adduct indicated that the BSSE is approximately 4.4 kcal mol^{-1}, resulting in about a 16% overestimate of the bond energy. The frequencies of the calculated IR bands have been scaled by 0.9613, in accordance with an earlier recommendation [82] for the B3LYP functional when used with the 6-31G* basis set. The absolute frequencies are still predicted too high, partly because the calculations were performed on PH_3 complexes in the gas phase, as opposed to PCy_3 complexes in *n*-hexane solution. However, the relative frequencies and intensities of the bands are in excellent agreement with our experimental results (see Table 3). The DFT calculations predict three ν(CO) bands and one ν(NN) mode at 2184 cm^{-1} for **W′**–N_2. However, the experimental ν(NN) data for **W**–N_2 suggest the presence of two overlapping bands at 2113 and 2117 cm^{-1}. This indicates the possibility of the existence of different coordination modes for the dinitrogen complex in solution. The end-on dinuclear complex, $W(CO)_3(P^iPr_3)_2$–N_2–$W(CO)_3(P^iPr_3)_2$ has been isolated and characterized by single crystal X-ray diffraction [63]. However, ν(NN) and mixed ν(NN)/ν(CO) modes were observed at 1939 and 1996 cm^{-1}, respectively for this compound, which are quite different to our experimental observation for **W**–N_2. In addition, involvement of a dimeric species is unlikely, since the formation rate constant of **W**–N_2 remained the same when we changed the laser intensity in our flash photolysis experiments. Therefore, for comparison we carried out a DFT calculation on the side-on bound mononuclear dinitrogen complex (where the N–N bond is parallel to the P–W–P bond axis). Since the calculated energy of this complex was found to be 16.1 kcal mol^{-1} higher than that calculated for the end-on mononuclear dinitrogen complex, the presence of such a species is extremely unlikely. Therefore, the shoulder observed on the

Table 3
Gas-phase DFT calculated bond energy (kcal mol^{-1}), orbitals, bond distances (Å), and IR frequencies (cm^{-1}) for **W′** and **W′**–N_2 complexes, together with the experimentally observed IR frequencies for **W** and **W**–N_2 in *n*-hexane solution

Properties	**W′**	**W′**–N_2
W–N_2 bond energy	–	25.7
HOMO[a]	$d_\pi + (mer - CO\ \pi^*)$	$d_\pi + (N_2\pi^* + mer - CO\ \pi^*)$
LUMO	d_{z^2} + *trans*-COπ^*	$N_2\pi^*$ + *mer*,*trans* − CO π^*
W–N_2 distance	–	2.110
N–N distance	–	1.121
ν(CO)[b]	1898(38), 1919(91), 1999(1)	1934(9), 1938(5), 2006(1)
ν(NN)	–	2184(2)
Exptl. ν(CO)[c]	1819m, 1837s, 1949w	1853s, 1857sh, 1953w
Exptl. ν(NN)[d]	–	2113w, 2117w

[a] The orbitals in parentheses are minor characters.
[b] Relative intensities in parentheses.
[c] For **W** and **W**–N_2 in *n*-hexane.
[d] For **W**–N_2 in *n*-hexane, s: strong; m: medium; w: weak; sh: shoulder.

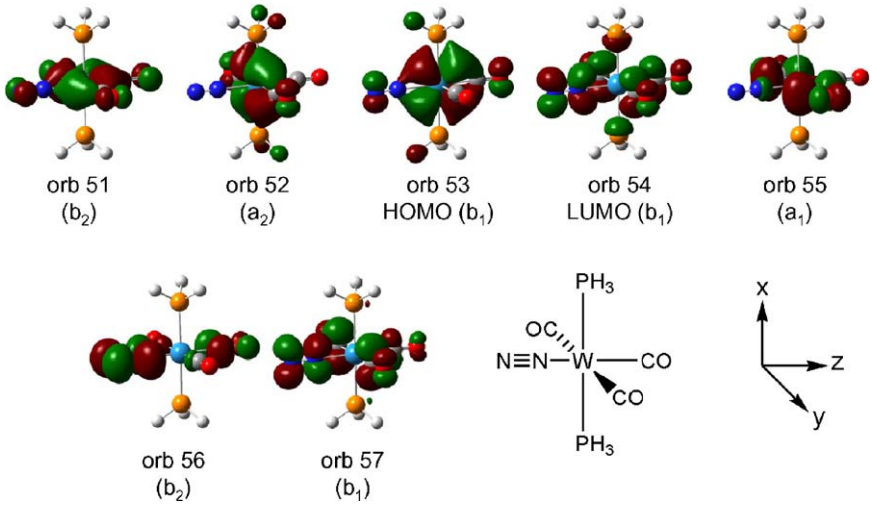

Fig. 6. DFT calculated frontier molecular orbitals of *mer*,*trans*-$W(CO)_3(PH_3)_2(N_2)$. For clarity, the orientation of the molecule in these diagrams is also shown, together with the cartesian axes used.

ν(NN) stretching band of **W**–N_2 could possibly be attributed to either an overtone or a combination band, although from the results of our calculations we cannot identify likely candidates.

The results of the DFT calculations on **W′** show that the HOMO is mainly an overlap of the W d_{xz} orbital (where the *xz*-plane contains the P–W–P(*x*) and *mer*-CO(*z*) axes: *z* is the C_2 symmetry axis) and the π_x^* orbital of the *mer*-CO, giving rise to a W–C π bond. The LUMO is largely an overlap of the W d_{z^2} orbital with the π_z^* orbitals of both *trans*-CO ligands, leading to a large lobe in the vacant coordination position. The LUMO + 1 is primarily composed of the π_x^* orbitals on the two *trans*-CO ligands. For **W′**–N_2, the HOMO is mainly an overlap of the W d_{xz} orbital with the π_x^* orbitals of the N_2 and *mer*-CO ligands, giving rise to W–N and W–C π_x bonds. The LUMO is largely located on the N_2 π_x^* and *mer*,*trans*-CO π_x^* orbitals, indicating that the W–N_2 bond can be easily photo-cleaved. The calculated frontier molecular orbitals for **W′**–N_2 are shown in Fig. 6. The lowest-energy transition is the HOMO to LUMO excitation mixed with HOMO − 2 to LUMO + 2 and HOMO to LUMO + 3 contributions at 380 nm, with an oscillator strength of 0.0480. The next lowest transition is the HOMO to LUMO + 1 at 367 nm with an oscillator strength of 0.0120. The LUMO + 1 is largely located on the π_y^* orbitals of the two *trans*-CO ligands. The third lowest transition is the HOMO − 1 to LUMO + 2 at 338 nm, with an oscillator strength of 0.0051. While the shape of the calculated spectrum for **W′**–N_2 matches well with the observed spectrum of **W**–N_2, the calculated absorptions are at slightly higher energies. More detailed calculations are currently underway, including calculations on the actual complexes used in our experiments, **W** and **W**–N_2. The results of these calculations will feature in an upcoming publication [69].

3. Conclusions and outlook

Kinetic studies of the photoinduced formation of transition metal–dinitrogen complexes using time-resolved infrared and UV–vis spectroscopy at room temperature, in both the gas phase and in solution have been summarized. Reactions of transition metal complex fragments with dinitrogen in the gas phase are typically much faster than those in solution, since the photogenerated fragments are coordinatively unsaturated and extremely reactive, with no interference from a solvent. Whereas in solution, solvent molecules generally behave as weak "token" ligands [10], interacting on the femto- to picosecond timescale [11] with the vacant coordination sites of unsaturated intermediates. Thus, the interaction with N_2 and the formation of a metal–dinitrogen bond tends to be slower in solution, due to the necessary displacement of a solvent molecule from the metal coordination sphere, coupled with the inherently lower diffusion rate in solution. However, many other factors such as metal oxidation state, spin multiplicity, and the size of the metal center, as well as steric and electronic effects of the peripheral ligands, can have a significant influence on the rate of N_2 binding and the structure and reactivity of the N_2 complex. This is demonstrated graphically in Fig. 7, which logarithmically compares the second-order rate constants observed for the reactions of various photogenerated intermediates with dinitrogen to generate the corresponding dinitrogen complexes, both in solution and in the gas phase at room temperature. In the gas phase, the major factor determining the rate of dinitrogen binding is the spin state of the metal center, since there is typically no activation barrier for this process. The difference in rate constant between a spin-allowed and a spin-disallowed binding step, for similar reacting species, can be up to three orders of magnitude. One exception is the reaction of $Fe(CO)_3(N_2)$ with N_2 in the gas phase [33], which was found to have a significant activation barrier of 5.7 ± 3.6 kcal mol^{-1}, causing the rate constant to drop considerably, to a value that is even low for a solution phase reaction. *mer*,*trans*-$W(CO)_3(PCy_3)_2$ (**W**) was found to react relatively slowly with N_2 in solution, most likely because of a fluxional internal agostic (W–H–C) interaction with the bulky cyclohexyl groups of the PCy_3 ligands and a possible interaction of the tungsten center with the solvent. This agostic "competition" for **W** between the ligand and solvent is currently under investigation.

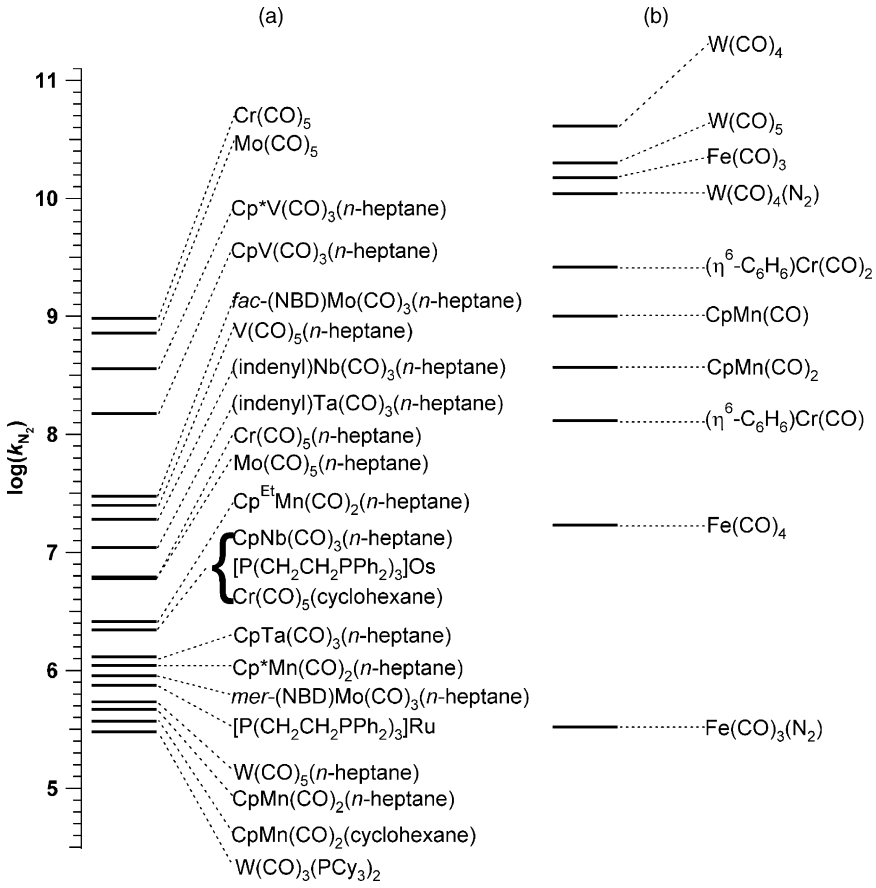

Fig. 7. Plots of log (k_{N_2}), where k_{N_2} ($M^{-1}\,s^{-1}$) are the second-order rate constants for the reaction of various photogenerated transition metal intermediate species with dinitrogen to form the corresponding dinitrogen complexes at room temperature in (a) solution and (b) the gas phase. See main text for references. In the cases where the intermediate species is solvated by a molecule of solvent, reaction with dinitrogen involves a substitution of the solvent molecule by N_2. In all other cases, the reaction involves a simple addition of N_2 to the intermediate. Cp: (η^5-C_5H_5); Cp^*: (η^5-C_5Me_5); Cp^{Et}: (η^5-C_5Et_5); indenyl: (η^5-C_9H_7); Cy: cyclohexyl; NBD: norbornadiene.

$CpM(CO)_2$(alkane) complexes (M = Mn and Re) have previously been shown to exhibit an unusually low reactivity toward CO in solution, when compared to other early transition metal alkane complexes [83,84]. Indeed, $CpRe(CO)_2$(cyclopentane) is the least reactive transition metal–alkane complex that has been observed in solution at room temperature [52]. This observation appears to hold true for reaction with dinitrogen, with the $CpMn(CO)_2$(alkane) complexes being the least reactive toward dinitrogen binding of all the solvated transient complexes that have so far been investigated [16,53] (see Fig. 7). Furthermore, recent data has revealed that $CpRe(CO)_2$(*n*-heptane) is considerably less reactive toward dinitrogen binding, with a rate constant, $k_{N_2} = 3.0 \times 10^3\,M^{-1}\,s^{-1}$($\log(k_{N_2}) = 3.48$) for the formation of $CpRe(CO)_2(N_2)$ in *n*-heptane [85]. The remaining transition metal complexes that have been studied in solution show a gradual increase in reactivity toward dinitrogen binding, similar to previously observed trends in the reactivity of these complexes toward CO [52,83,84,86]. Thus, upon moving from group 7 to group 5 and from the third to first row, the reactivity increases dramatically. One exception is the much higher reactivity of *fac*-$(NBD)Mo(CO)_3$(*n*-heptane) toward N_2 binding compared to *mer*-$(NBD)Mo(CO)_3$(*n*-heptane) [49]. This was attributed to a weakening of the Mo-heptane interaction in the *fac* configuration caused by steric and electronic effects. Furthermore, an increase in the steric bulk of the peripheral ligands in a similar set of complexes has been shown to cause an increase in the reactivity of the solvated intermediate species toward N_2, due to increased interactions with, and thus a weakening of, the metal–solvent bond [53]. The most reactive complexes toward dinitrogen binding that have been studied in solution are $M(CO)_5$ (M = Cr and W) in perfluoromethylcyclohexane [43]. Their remarkably high reactivity is due to the fact that, unlike in conventional solvents, the perfluoroalkane solvent is practically non-coordinating. Thus, the photogenerated $M(CO)_5$ intermediates are virtually "naked" unsaturated species and there is very little barrier for their reaction with dinitrogen other than diffusion. The W–N_2 bond in *mer*,*trans*-$W(CO)_3(PCy_3)_2(N_2)$ is sterically protected by the bulky cyclohexyl groups and the adduct lives for many days in a sealed vessel. This is in contrast to other dinitrogen complexes that do not possess such bulky ligands, for example, $Cr(CO)_5(N_2)$ and $CpM(CO)_3(N_2)$ (M = V, Nb and Ta), which decay within seconds in solution at room temperature [30,55,56].

Time-resolved spectroscopic studies of M–N_2 bond formation by us and others clearly demonstrate that TRIR spectroscopy is a powerful tool for identifying transient intermediates, for

elucidating the structures and binding modes of these intermediates and products, and for the determination of reaction pathways and kinetics. The facile observation of a bound dinitrogen ν(NN) IR stretching frequency with the **W**–N_2 system and others [30,56], provides a unique opportunity to extend the technique in future kinetic and mechanistic investigations of N_2 activation by protons and photoinduced electrons, with complexes that do not possess conventional IR reporter ligands such as CO. Furthermore, TRIR spectroscopy complements flash photolysis, which provides electronic information on intermediates and extremely accurate decay kinetics. Parallel to experimental investigations, theoretical studies will play an increasingly important role for confirming vibrational and UV–vis spectral assignments, identifying the most stable conformers, and understanding the energetics of the reaction mechanisms involved in catalytic chemical nitrogen fixation cycles.

Acknowledgments

We thank Prof. M.W. George for the provision of unpublished data. This work was performed at Brookhaven National Laboratory, funded under contract DE-AC02-98CH10886 with the U.S. Department of Energy and supported by its Division of Chemical Sciences, Office of Basic Energy Sciences. K.-W.H. acknowledges a Gertrude and Maurice Goldhaber Distinguished Fellowship.

References

[1] A.D. Allen, C.V. Senoff, Chem. Commun. (London) (1965) 621.
[2] J. Chatt, J.R. Dilworth, R.L. Richards, Chem. Rev. 78 (1978) 589.
[3] M. Hidai, Y. Mizobe, Chem. Rev. 95 (1995) 1115.
[4] M. Hidai, Coord. Chem. Rev. 185–186 (1999) 99.
[5] M.D. Fryzuk, S.A. Johnson, Coord. Chem. Rev. 200–202 (2000) 379.
[6] B.K. Burgess, D.J. Lowe, Chem. Rev. 96 (1996) 2983.
[7] J.R. Jennings (Ed.), Catalytic Ammonia Synthesis: Fundamentals and Practice, Plenum Press, New York, 1991.
[8] J.K. Burdett, Coord. Chem. Rev. 27 (1978) 1.
[9] R.B. Hitam, K.A. Mahmoud, A.J. Rest, Coord. Chem. Rev. 55 (1984) 1.
[10] G.R. Dobson, P.M. Hodges, M.A. Healy, M. Poliakoff, J.J. Turner, S. Firth, K.J. Asali, J. Am. Chem. Soc. 109 (1987) 4218.
[11] X.L. Xie, J.D. Simon, J. Am. Chem. Soc. 112 (1990) 1130.
[12] R.N. Perutz, Pure Appl. Chem. 70 (1998) 2211.
[13] R.G.W. Norrish, G. Porter, Nature (London) 164 (1949) 658.
[14] F.C. De Schryver, S. De Feyter, G. Schweitzer (Eds.), Femtochemistry, Wiley-VCH, Weinheim, 2001.
[15] K. McFarlane, B. Lee, J. Bridgewater, P.C. Ford, J. Organomet. Chem. 554 (1998) 49.
[16] B.S. Creaven, A.J. Dixon, J.M. Kelly, C. Long, M. Poliakoff, Organometallics 6 (1987) 2600.
[17] D.C. Grills, M.W. George, in: J.M. Chalmers, P.R. Griffiths (Eds.), Handbook of Vibrational Spectroscopy, vol. 1, John Wiley and Sons Ltd., Chichester, 2002, p. 677.
[18] M.W. George, M. Poliakoff, J.J. Turner, Analyst 119 (1994) 551.
[19] W. Uhmann, A. Becker, C. Taran, F. Siebert, Appl. Spectrosc. 45 (1991) 390.
[20] R.A. Palmer, J.L. Chao, R.M. Dittmar, V.G. Gregoriou, S.E. Plunkett, Appl. Spectrosc. 47 (1993) 1297.
[21] P.Y. Chen, R.A. Palmer, Appl. Spectrosc. 51 (1997) 580.
[22] G.D. Smith, R.A. Palmer, in: J.M. Chalmers, P.R. Griffiths (Eds.), Handbook of Vibrational Spectroscopy, vol. 1, John Wiley and Sons Ltd., Chichester, 2002, p. 625.
[23] X.Z. Sun, S.M. Nikiforov, J.X. Yang, C.S. Colley, M.W. George, Appl. Spectrosc. 56 (2002) 31.
[24] K. Iwata, H. Hamaguchi, Appl. Spectrosc. 44 (1990) 1431.
[25] T. Yuzawa, C. Kato, M.W. George, H.O. Hamaguchi, Appl. Spectrosc. 48 (1994) 684.
[26] Y.H. Wang, T. Yuzawa, H.O. Hamaguchi, J.P. Toscano, J. Am. Chem. Soc. 121 (1999) 2875.
[27] M. Hashimoto, T. Yuzawa, C. Kato, K. Iwata, H. Hamaguchi, in: J.M. Chalmers, P.R. Griffiths (Eds.), Handbook of Vibrational Spectroscopy, vol. 1, John Wiley and Sons Ltd., Chichester, 2002, p. 666.
[28] Y. Ishikawa, P.A. Hackett, D.M. Rayner, J. Phys. Chem. 93 (1989) 652.
[29] Y. Ishikawa, P.A. Hackett, D.M. Rayner, J. Phys. Chem. 92 (1988) 3863.
[30] S.P. Church, F.W. Grevels, H. Hermann, K. Schaffner, Inorg. Chem. 23 (1984) 3830.
[31] R.C. Reid, J.M. Prausnitz, T.K. Sherwood, The Properties of Gases and Liquids, 3rd ed., McGraw-Hill, New York, 1977.
[32] P.G. House, E. Weitz, Chem. Phys. Lett. 266 (1997) 239.
[33] J. Wang, G.T. Long, E. Weitz, J. Phys. Chem. A 105 (2001) 3765.
[34] T.A. Seder, A.J. Ouderkirk, E. Weitz, J. Chem. Phys. 85 (1986) 1977.
[35] R.J. Ryther, E. Weitz, J. Phys. Chem. 95 (1991) 9841.
[36] P.G. House, E. Weitz, J. Phys. Chem. A 101 (1997) 2988.
[37] E. Weitz, J. Phys. Chem. 98 (1994) 11256.
[38] Y.F. Zheng, W.H. Wang, J.G. Lin, Y.B. She, K.J. Fu, J. Phys. Chem. 96 (1992) 9821.
[39] J.K. Burdett, A.J. Downs, G.P. Gaskill, M.A. Graham, J.J. Turner, R.F. Turner, Inorg. Chem. 17 (1978) 523.
[40] J.J. Turner, M.B. Simpson, M. Poliakoff, W.B. Maier II, J. Am. Chem. Soc. 105 (1983) 3898.
[41] J.J. Turner, M.B. Simpson, M. Poliakoff, W.B. Maier II, M.A. Graham, Inorg. Chem. 22 (1983) 911.
[42] S.M. Howdle, M.A. Healy, M. Poliakoff, J. Am. Chem. Soc. 112 (1990) 4804.
[43] J.M. Kelly, C. Long, R. Bonneau, J. Phys. Chem. 87 (1983) 3344.
[44] R. Bonneau, J.M. Kelly, J. Am. Chem. Soc. 102 (1980) 1220.
[45] E. Wilhelm, R. Battino, Chem. Rev. 73 (1973) 1.
[46] The diffusion-controlled rate constant, k_d in perfluoromethylcyclohexane was calculated from the relationship, $k_d = 8RT/3\eta$ using the viscosity, $\eta = 1.56 \times 10^{-3}$ Pa s that was reported in R.N. Haszeldine, F. Smith, J. Chem. Soc. (1951) 603.
[47] S.P. Church, F.W. Grevels, H. Hermann, K. Schaffner, J. Chem. Soc., Chem. Commun. (1985) 30.
[48] S.A. Jackson, P.M. Hodges, M. Poliakoff, J.J. Turner, F.W. Grevels, J. Am. Chem. Soc. 112 (1990) 1221.
[49] P.M. Hodges, S.A. Jackson, J. Jacke, M. Poliakoff, J.J. Turner, F.W. Grevels, J. Am. Chem. Soc. 112 (1990) 1234.
[50] B.S. Creaven, M.W. George, A.G. Ginzburg, C. Hughes, J.M. Kelly, C. Long, I.M. McGrath, M.T. Pryce, Organometallics 12 (1993) 3127.
[51] C.J. Breheny, J.M. Kelly, C. Long, S. O'Keefe, M.T. Pryce, G. Russell, M.M. Walsh, Organometallics 17 (1998) 3690.
[52] G.I. Childs, C.S. Colley, J. Dyer, D.C. Grills, X.Z. Sun, J.X. Yang, M.W. George, J. Chem. Soc., Dalton Trans. (2000) 1901.
[53] F.P.A. Johnson, M.W. George, V.N. Bagratashvili, L.N. Vereshchagina, M. Poliakoff, Mendeleev Commun. (1991) 26.
[54] F.P.A. Johnson, V.K. Popov, M.W. George, V.N. Bagratashvili, M. Poliakoff, J.J. Turner, Mendeleev Commun. (1991) 145.
[55] M.W. George, M.T. Haward, P.A. Hamley, C. Hughes, F.P.A. Johnson, V.K. Popov, M. Poliakoff, J. Am. Chem. Soc. 115 (1993) 2286.
[56] G.I. Childs, D.C. Grills, S. Gallagher, T.E. Bitterwolf, M.W. George, J. Chem. Soc., Dalton Trans. (2001) 1711.
[57] R. Osman, D.I. Pattison, R.N. Perutz, C. Bianchini, J.A. Casares, M. Peruzzini, J. Am. Chem. Soc. 119 (1997) 8459.
[58] G.J. Kubas, R.R. Ryan, B.I. Swanson, P.J. Vergamini, H.J. Wasserman, J. Am. Chem. Soc. 106 (1984) 451.
[59] G.J. Kubas, Acc. Chem. Res. 21 (1988) 120.
[60] G.J. Kubas, J. Organomet. Chem. 635 (2001) 37.
[61] G.J. Kubas, Metal Dihydrogen and σ-Bond Complexes: Structure, Theory, and Reactivity, Kluwer Academic/Plenum Press, New York, 2001.

[62] H.J. Wasserman, G.J. Kubas, R.R. Ryan, J. Am. Chem. Soc. 108 (1986) 2294.
[63] M.D. Butts, J.C. Bryan, X.L. Luo, G.J. Kubas, Inorg. Chem. 36 (1997) 3341.
[64] K. Zhang, A.A. Gonzalez, C.D. Hoff, J. Am. Chem. Soc. 111 (1989) 3627.
[65] A.A. Gonzalez, K. Zhang, S.P. Nolan, R.L. Delavega, S.L. Mukerjee, C.D. Hoff, G.J. Kubas, Organometallics 7 (1988) 2429.
[66] A.A. Gonzalez, K. Zhang, C.D. Hoff, Inorg. Chem. 28 (1989) 4285.
[67] T. Hamada, B.S. Brunschwig, E. Eifuku, E. Fujita, M. Korner, S. Sasaki, R. van Eldik, J.F. Wishart, J. Phys. Chem. A 103 (1999) 5645.
[68] D.W. Thompson, J.F. Wishart, B.S. Brunschwig, N. Sutin, J. Phys. Chem. A 105 (2001) 8117.
[69] D.C. Grills, R. van Eldik, J.T. Muckerman, E. Fujita, in prepration.
[70] M.J. Frisch, G.W. Trucks, H.B. Schlegel, G.E. Scuseria, M.A. Robb, J.R. Cheeseman, V.G. Zakrzewski, J.A.M. Jr., R.E. Stratmann, J.C. Burant, S. Dapprich, J.M. Millam, A.D. Daniels, K.N. Kudin, M.C. Strain, O. Farkas, J. Tomasi, V. Barone, M. Cossi, R. Cammi, B. Mennucci, C. Pomelli, C. Adamo, S. Clifford, J. Ochterski, G.A. Petersson, P.Y. Ayala, Q. Cui, K. Morokuma, N. Rega, P. Salvador, J.J. Dannenberg, D.K. Malick, A.D. Rabuck, K. Raghavachari, J.B. Foresman, J. Cioslowski, J.V. Ortiz, A.G. Baboul, B.B. Stefanov, G. Liu, A. Liashenko, P. Piskorz, I. Komaromi, R. Gomperts, R.L. Martin, D.J. Fox, T. Keith, M.A. Al-Laham, C.Y. Peng, A. Nanayakkara, M. Challacombe, P.M.W. Gill, B. Johnson, W. Chen, M.W. Wong, J.L. Andres, C. Gonzalez, M. Head-Gordon, E.S. Replogle, J.A. Pople, Gaussian 03, Revision C.02, Wallingford, CT, 2004.
[71] P.J. Hay, W.R. Wadt, J. Chem. Phys. 82 (1985) 270.
[72] W.R. Wadt, P.J. Hay, J. Chem. Phys. 82 (1985) 284.
[73] P.J. Hay, W.R. Wadt, J. Chem. Phys. 82 (1985) 299.
[74] R. Ditchfie, W.J. Hehre, J.A. Pople, J. Chem. Phys. 54 (1971) 724.
[75] W.J. Hehre, R. Ditchfie, J.A. Pople, J. Chem. Phys. 56 (1972) 2257.
[76] P.C. Harihara, J.A. Pople, Theor. Chim. Acta 28 (1973) 213.
[77] A.D. Becke, Phys. Rev. A 38 (1988) 3098.
[78] C. Lee, W. Yang, R.G. Parr, Phys. Rev. B 37 (1988) 785.
[79] A.D. Becke, J. Chem. Phys. 98 (1993) 5648.
[80] E. Fujita, B.S. Brunschwig, C. Creutz, J.T. Muckerman, N. Sutin, D. Szalda, R. van Eldik, Inorg. Chem. (2006) ASAP article. http://dx.doi.org/10.1021/ic0515498.
[81] G.J. Kubas, C.J. Unkefer, B.I. Swanson, E. Fukushima, J. Am. Chem. Soc. 108 (1986) 7000.
[82] M.W. Wong, Chem. Phys. Lett. 256 (1996) 391.
[83] X.Z. Sun, D.C. Grills, S.M. Nikiforov, M. Poliakoff, M.W. George, J. Am. Chem. Soc. 119 (1997) 7521.
[84] G.I. Childs, D.C. Grills, X.Z. Sun, M.W. George, Pure Appl. Chem. 73 (2001) 443.
[85] Unpublished data privately communicated by Prof. M. W. George, School of Chemistry, University of Nottingham, UK.
[86] D.C. Grills, X.Z. Sun, G.I. Childs, M.W. George, J. Phys. Chem. A 104 (2000) 4300.